Why do pens have rubbery grips?

Adams, Michael; Dzidek, Brygida; Bochereau, Serena; Johnson, Simon; Hayward, Vincent

DOI:
10.1073/pnas.1706233114

Document Version
Peer reviewed version

Citation for published version (Harvard):
Adams, M, Dzidek, B, Bochereau, S, Johnson, S & Hayward, V 2017, 'Why do pens have rubbery grips?', *National Academy of Sciences. Proceedings*, vol. 114, no. 41, pp. 10864-10869.
https://doi.org/10.1073/pnas.1706233114

Why do pens have rubbery grips?

Brygida Dzidek [*], Séréna Bochereau [†], Simon Johnson [‡], Vincent Hayward [†], and Michael Adams [*]

[*]School of Engineering, University of Birmingham, Birmingham B15 2TT, UK,[†]Sorbonne Universités, UPMC Univ Paris 06, ISIR, F-75005, Paris, France, and [‡]Unilever R&D Port Sunlight, Bebington, Wirral CH63 3JW, UK

Submitted to Proceedings of the National Academy of Sciences of the United States of America

The process by which human fingers gives rise to stable contacts with smooth, hard objects is surprisingly slow. Using high-resolution imaging we found that, when pressed against glass, the actual contact made by finger pad ridges evolved over time following a first-order kinetics relationship. This evolution was the result of a two-stage coalescence process of microscopic junctions made between the keratin of the *stratum corneum* of the skin and the glass surface. This process was driven by the secretion of moisture from the sweat glands since increased hydration in *stratum corneum* caused it to become softer. Saturation was typically reached within twenty seconds of loading the contact regardless of the initial moisture state of the finger and of the normal force applied. Hence, the gross contact area, frequently used as a benchmark quantity in grip and perceptual studies, is a poor reflection of the actual contact mechanics that take place between human fingers and smooth, impermeable surfaces. In contrast, the formation of a steady state contact area is almost instantaneous if the counter surface is soft relative to keratin in a dry state. It is for this reason that elastomers are commonly employed to coat grip surfaces.

Finger friction | True contact area kinetics | Biotribology | Fingerprints

Abbreviations: PDMS, polydimethylsiloxane; FTIR, frustrated total internal reflection

Introduction

We often take it for granted that our fingers instantly bring about continuous contact when they touch smooth objects. The fingerprint marks remaining on these objects after detachment, however, are the record of a surprisingly slow process. During a period of many seconds, several phenomena take place at different length and time scales that eventually lead to a stable contact state where the flattened apices of the ridges establish a uniform contact with the counter surface. Here we observed that the so-called 'true contact area', which quantifies the amount of material in intimate contact, i.e in atomic proximity [1, 2], varies dynamically over a period of many seconds whilst the apparent, or gross, contact area, by and large, remains unchanged through time.

A knowledge of the evolution of a contact is informative because a true contact area determines the creation of friction, which is so essential to everyday life. Without a large true contact area made by our hands, it would be nearly impossible to lift a glass or to hold onto a handrail in a transport vehicle. Recent tactile display technologies depend crucially on the development of friction between a finger and a glass surface [3, 4]. Some powerful tactile illusions are the direct consequence of the differential frictional properties of surfaces across space [5] and astonishing human perceptual performance in the discrimination of materials can be explained by subtle variations in frictional properties [6]. Thus there is ample motivation for investigating the details of the formation of the true contact area by fingertips in contact with smooth surfaces.

The superficial layer of human finger pads that is in direct contact with objects, termed the *stratum corneum*, is made in a large proportion of keratin (keratinised cells), one of the most abundant structural material in animals. The keratin of the *stratum corneum* is a composite material that comprises a mix of molecules in a crystalline state and those in an amorphous state. The crystalline component is impervious to the effect of water so it can preserve its gross shape. The amorphous component, however, is avid of water and the presence or absence of water profoundly modifies its mechanical properties [7]. Dry *stratum corneum* has an elastic modulus of about 1 GPa but this value can be reduced by approximatively four orders-of-magnitude when it is saturated with water [8]. In the wet state, *stratum corneum* can yield 150% of its original length at almost constant stress, giving it plasticity [9].

The macroscopic geometry of the finger pad, which is characterised by ridges and valleys that compress, decompress, and stretch during interactions with surfaces, undergoes considerable gross deformation even for moderate contact loads [10]. The surface of the ridges exhibit roughly cylindrical cross sections and are separated by valleys [8]. They form loops, whorls, or arch patterns that are unique to each individual. The evolution of the apparent area of contact arising from the deformation of a finger pad has been examined using optical imaging during incipient slip [11], at different force levels [12, 13], at different moisture contents [14] and tangential loads leading to slip [15], under rotation and lateral sliding movements over flat, raised or indented glass surfaces [10], during stick-to-slip transitions in distal, proximal, radial and ulnar directions [16], over complete stick-to-slip epochs [17], and under the effects of oscillating loads [18, 19].

Previous studies considered the area of a finger pad contact macroscopically. A contact was typically described by an apparent, or gross area, and then by excluding the interstitial spaces between the ridges in an effort to better approximate the true contact area. Thus, the total contact area made by the ridges compared to the gross area would quantify their

Significance

Why does gripping a pen, tool or handle feel more secure when it is coated with a rubbery material? The keratin of the outer layer of the skin is stiff and rough at a small scale. When encountering a smooth, stiff, and impermeable surface such as shiny plastic, polished metal or glass, the actual contact area is initially small and hence so is the friction. Because the keratin softens slowly when it is hydrated by the moisture secreted from the sweat pores, it requires many seconds for the contact area to increase to the value reached almost instantaneously with a soft material such as a rubber. This mechanism might also be used by our tactile sense to identify materials and has implications for the design of tactile displays.

Reserved for Publication Footnotes

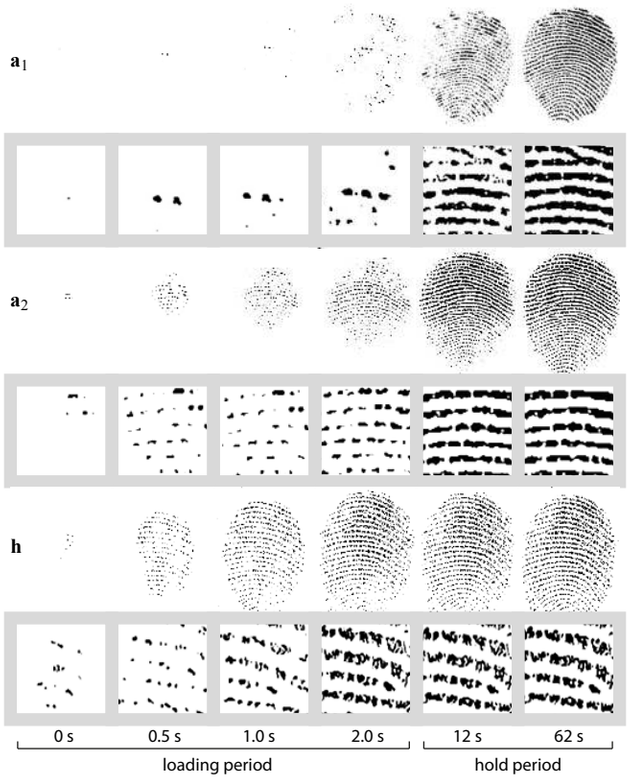

Fig. 1. Temporal evolution of the contact area on a glass surface for participant A corresponding to trials $\mathbf{a}_1$ and $\mathbf{a}_2$ (see Table 1). Each row is associated with framed enlarged image portions depicting the creation, growth, and coalescence of regions of the junction area. The last two rows show the contact evolution on a PDMS surface under similar conditions for participant B; data set **h**.

overall deformation since these two values would coincide if the ridges were completely deformed.

The ridges themselves are far from being smooth and exhibit small-scale topographical features. In a recent study, [20] the effect of these features could be, for the first time, observed directly. They initially yielded few unconnected regions within the ridge contacts. The summed areas of these regions, which were described as junctions, corresponded to a total area denoted, A_{junct}. The total junction contact area was observed to grow for many seconds during the holding period following a loading event, while the gross and ridge areas, A_{gross} and A_{ridge} respectively, remained unchanged [20]. This growth was the result of a two-step coalescence process such that the number of junctions, N, first increased, followed by their expansion that led to a rise in connectivity. It was surmised that this process was the result of an occlusion mechanism such that the *stratum corneum* became gradually plasticised under the action of moisture secreted from the many sweat pores located in the ridges. This phenomenon could explain the first-order growth kinetics exhibited by the coefficient of friction [2].

We investigated this newly discovered phenomenon in greater detail by characterising the influence of the loading forces and the loading rate on its time course. The present study provides a basis for establishing a robust description of the evolution of the contact area for steady pressing conditions associated with everyday interactions involving smooth surfaces. The results are contrasted with the case of a contact of a finger pad with an elastomer. With such a counter surface, the kinetics of contact formation exhibit a drastically different behaviour since its relative softness allows a steady state contact to be reached almost instantaneously.

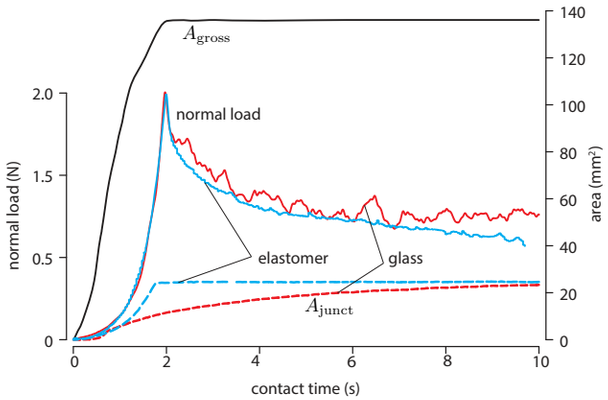

Fig. 2. Typical evolution of the load force, A_{gross} and A_{junct} as a function of contact time for a glass (red) and for an elastomer (blue) counter surface. The evolution of A_{gross} does not depend on the material.

The observed contact evolutions during interactions with solid surfaces is a tribute to the ability of the human nervous system to secure stable grips and to achieve tactile perceptual constancy despite the extensive variations in detailed contact mechanics through time during finger contact with objects. They also have important implications for the design of touch screens with haptic feedback that rely on the modulation of friction to provide computer-controlled sensations.

Results

Fingerprint images for two participants were obtained using the technique of Frustrated Total Internal Reflection (*Methods*). The washed and dried pads of their index fingers were slowly pressed against the face of a prism until reaching a maximum normal loading force. The fingers were then held in a fixed isometric condition for 60 s once the maximum normal load was reached. Testing conditions differed by rate of compression, maximum normal load, counter surface material, and participant. Binary images obtained after enhancement and thresholding (*Methods*) are exemplified in Fig. 1 for different instants after the initial contact. Enlarged image portions more clearly show how the junctions evolved with time. Figures 2 and 3 show the results of an automated image analysis procedure performed at high resolution (*Methods*).

Conditions. There were eight testing conditions labeled from **a** to **h** listed in Table 1. Condition **h** corresponded to the finger of participant B pressing against a sheet of PDMS, a silicone-based transparent elastomer (*Methods*). Trials carried out with a same finger tested twice under the same condition have subscripts 1 and 2. Compression rates were 0.5, 1.0, or 2.0 mm s^{-1} and the maximum normal forces were 1.0 or 2.0 N. The time t_{max} was the time at which the maximum normal force was reached and A_{E} represented the relative contact area at the end of the hold period computed as A_{junct} normalised by A_{gross}. Fourteen data sets, see Table 1, were successfully acquired with very low likelihood that accidental lateral slips of the finger took place during imaging (*Methods*).

Table 1. Experimental protocol loading parameters. Subscripts in trial labels indicate repeated conditions. Results show the values of the best fit parameters to first-order kinetics [1]. Missing values indicate the absence of a good fit.

	conditions				results				
trials	rate ($\mathrm{mm\,s^{-1}}$)	load (N)	participant	material	A_0 ($\mathrm{mm^2}$)	A_∞ ($\mathrm{mm^2}$)	λ (s)	$t_{\max}$ (s)	A_E ($t = 60\,\mathrm{s}$)
$\mathbf{a}_1$	1.0	2.0	A	glass	3.7 ± 0.2	39.5 ± 0.2	16.5 ± 0.3	2.2	0.39
$\mathbf{a}_2$	1.0	2.0			20.9 ± 0.6	38.4 ± 0.2	5.5 ± 0.4	2.8	0.35
$\mathbf{b}_1$	1.0	3.0			19.5 ± 0.5	35.5 ± 0.1	3.2 ± 0.2	2.2	0.37
$\mathbf{b}_2$	1.0	3.0			29.5	–	–	2.4	0.39
$\mathbf{c}_1$	2.0	2.0			4.0 ± 0.9	29.3 ± 1.9	27.0 ± 3.1	1.2	0.30
$\mathbf{c}_2$	2.0	2.0			4.3 ± 0.2	30.9 ± 0.2	11.2 ± 0.3	1.0	0.31
$\mathbf{d}_1$	0.5	2.0	B	glass	0.7	–	–	3.4	0.01
$\mathbf{d}_2$	0.5	2.0			1.9	–	–	3.3	0.09
$\mathbf{e}_1$	1.0	2.0			7.4 ± 0.4	26.7 ± 0.4	16.2 ± 1.1	1.4	0.27
$\mathbf{e}_2$	1.0	2.0			15.0 ± 0.6	38.6 ± 0.5	15.6 ± 1.3	1.7	0.37
$\mathbf{f}_1$	1.0	3.0			2.6	–	–	1.7	0.17
$\mathbf{f}_2$	1.0	3.0			9.3 ± 0.4	29.1 ± 0.4	16.0 ± 0.1	1.8	0.25
$\mathbf{g}$	2.0	2.0			8.0 ± 0.7	28.2 ± 0.3	9.5 ± 0.8	0.8	0.28
$\mathbf{h}$	1.0	2.0	B	PDMS	–	25.0	–	2.4	0.38

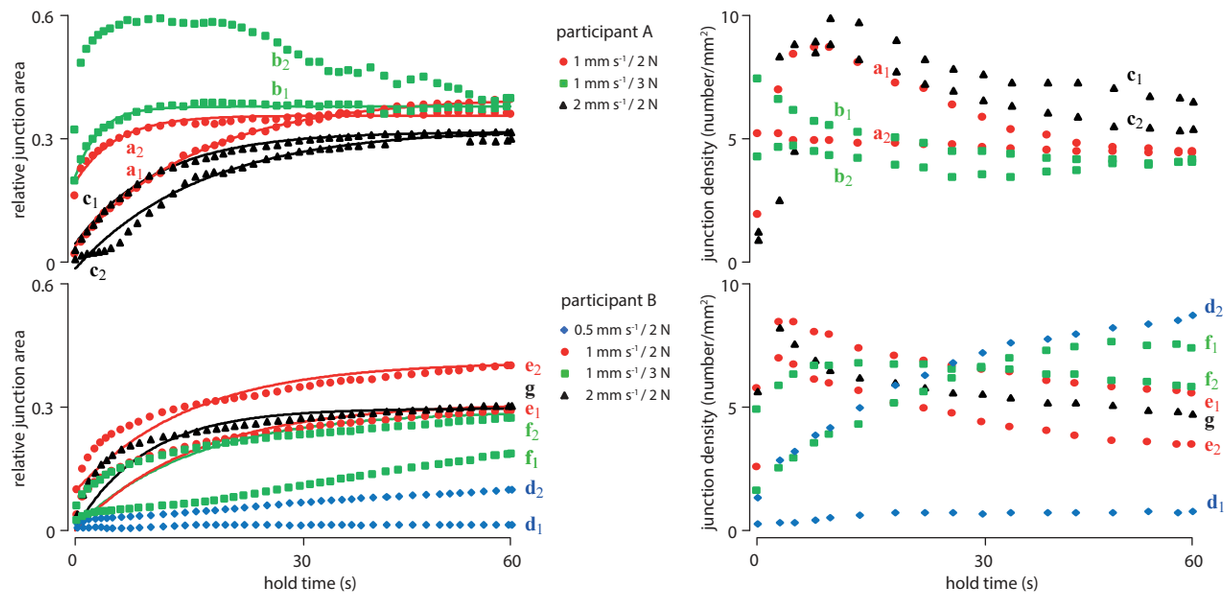

Fig. 3. Evolution of the relative junction area $A_\mathrm{E} = A_\mathrm{junct}/A_\mathrm{gross}$ and of the junction density, N/A_gross, as a function of hold time in contact with glass for participants A and B and for a range of loading rates and applied loads. Solid lines show first-order kinetics best fits.

Junction area kinetics. Figure 2 shows the typical evolution of A_junct as a function of contact time with glass. During the loading period, the value of A_gross increased to a maximum while the value of A_junct increased during the loading and the hold periods. During the hold period at constant compression, the normal force relaxed to less than half its initial value because of the viscoelastic properties of finger tissues [21].

Figure 3 shows the temporal evolution of A_E and of the junction density, N/A_gross, as a function of the hold time, t, for the fourteen trials. With the exception of trials $\mathbf{d}_1$, $\mathbf{d}_2$, $\mathbf{f}_1$, and $\mathbf{b}_2$, A_junct increased relative to A_gross at a decreasing rate such that the data could be adequately described by a first-order kinetics equation,

$$A_\mathrm{junct}(t) = A_\infty + (A_0 - A_\infty)\exp\left(-\frac{t}{\lambda}\right), \qquad [1]$$

where λ is the characteristic time and where the subscripts 0 and ∞ refer to the values of A_junct at times $t = 0$ and $t \to \infty$.

Junction area and junction density kinetics. Fitting the parameters A_∞, A_0, and λ of [1] to the data gave the values indicated in Table 1. The smallest value of the coefficient of determination, R^2, was 0.93. In many cases, the junction density increased to a maximum value during the loading period and then gradually decreases to a stable value. For trials $\mathbf{d}_1$ and $\mathbf{d}_2$, however, the junction density continued to increase during the whole contact period. For the finger pressing against the elastomer surface the evolution of the effective contact area, A_E, was so rapid that the kinetics could not be observed. As a result, A_E closely tracked the evolution of the normal load, reaching its ultimate value once the load ceased to increase.

Discussion

Variability. Despite highly controlled testing conditions, there were very large differences in the evolution of the junction contact area between a fingertip and a hard smooth surface, such as glass. During trial $\mathbf{b}_2$, the normalised contact area, A_{E}, exhibited a large maximum value 10 s after the onset of the hold period, before decreasing to a steady value. The junction density increased during the loading period and then decreases to a stable value toward the end of the hold period.

For most trials, the evolution of the junction area followed a first-order kinetics relationship, the junction density tended to increase during the loading period and to decrease to a steady value near the end of the hold period. For some trials ($\mathbf{f}_1$, $\mathbf{d}_1$, $\mathbf{d}_2$), however, the effective contact area increased in a manner that could not be described by [**1**].

Role of plasticisation. During the loading period, A_{junct} and N naturally increased. The subsequent behaviour of these values during the hold period, however, depended on other factors than time, chief among them is the extent to which the *stratum corneum* became plasticised. Plasticisation, which is linked to a decrease of the elastic modulus, is caused by hydration and thus depends on pre-existing moisture before contact and on the rate of secretion of sweat from the pores.

For most trials, the reduction in the junction density during the hold period reflected the slow progress of a coalescence process until complete segments became connected. The changes occurred gradually over the hold period which suggests that the coalescence process was governed by the rate of transport of sweat from the pores and by subsequent diffusion into the *stratum corneum* layer. The eventual reduction of the junction contact area for trial $\mathbf{b}_2$ suggests that in this case the finger had a high initial level of hydration followed by evaporation of water within the interstitial ridge valleys.

Trial $\mathbf{d}_1$ is an example of a finger that was very dry, both at the onset of contact and subsequently, as can be seen from the very slow rise in the true contact area and in the junction density. It is nevertheless possible that microscopic junctions actually existed but were too small to be resolved.

Trials $\mathbf{d}_2$ and $\mathbf{f}_1$ corresponded to fingers that were relatively dry but the fact that the contact areas increased with the hold time suggests that the *stratum corneum* was more hydrated than in the case of $\mathbf{d}_1$. Moreover, these trials exhibited a continuous increase in the junction density that must have corresponded to junctions gradually being formed as a result of occlusion, but with insufficient moisture softening for junction coalescence to take place.

In complete contrast, variability was absent for the trials where a finger pressed onto an elastomeric counter surface, regardless of the state of hydration of the finger. This occurence is exemplified by trial $\mathbf{h}$. The junction area growth kinetics was so rapid that it could not be resolved by our apparatus.

Contact mechanics. As shown in Fig. 1, throughout the evolution of a finger contact against glass, the width of the junctions and of the ridge apices tended to be greater towards the centre of the contact area than in the periphery. These differences can be understood by applying Hertz theory at two different length scales, one at the scale of the whole finger and the other at the scale of individual ridges [8]. The images of the finger print ridges (see also, Fig. 4a) thus were generally less dense towards the periphery, which is consistent with a decrease of the Hertzian contact pressure. While it is not possible to distinguish between the effects of very narrow gaps and partial contact arising from surface roughness, *in vivo* confocal Raman spectroscopy of skin suggests that it is unlikely that the contacts observed optically involve thin moisture or air films [22].

The sweat pores caused small regions to remain without contact (white regions in Fig. 1). Thus, even for fully connected ridges, A_{true} was always smaller than A_{ridge}.

Tribology. The adhesion model of friction [23, 24], which has been shown to be applicable to the *stratum corneum* [27, 28], states that the frictional force, f_{f}, depends on the product of the interfacial shear strength, τ, and the true area of contact, A_{true}, which is reflected by A_{junct}. The true area of contact measures the amount of intimate, friction-generating contact. Such contacts have transient molecular junctions at the sliding interface.

The frictional force is the work done per unit of sliding distance required to rupture those junctions that transmit stress across the sliding interface and cause sub-surface inelastic deformation to a depth of about 100 nm [25]. For glassy polymers, the interfacial stress, determined by τ, has been related to surface yielding with values of 1 to 10 MPa that are about an order of magnitude smaller than those in the bulk since surface polymer chains have greater freedom to align with the sliding direction [25]. Plasticisation by water of hydrophilic polymers such as nylon is known to cause a reduction in τ in a similar way to that observed for the bulk yield stress [26].

Human fingerprint ridges are decorated with very small-scale surface topographical features that correspond to the asperities of rough surfaces. When compressed, the *stratum corneum* is initially stiff and the deformation of the asperities is limited. The increase in the area of existing junctions or ridges, and the consequent formation of new asperity contacts with increasing applied normal load, w, is the origin of Coulomb's law, $f_{\mathrm{f}} = \mu w$ where μ is the coefficient of friction. With time, the asperities become compliant because of the plasticisation by moisture and A_{true} increases. It is reasonable to believe that the *stratum corneum* behaves like nylon such that, concomitantly, the value of τ decreases as a result of the plasticisation. We can model this process by writing, $f_{\mathrm{f}} = \tau(t)A_{\mathrm{true}} = \tau(t)\phi(t)A_{\mathrm{junct}}(t \to \infty)$, where $A_{\mathrm{junct}}(t \to \infty)$ is the steady state contact area of the junctions, including those that have coalesced to form whole ridge segments. The scalar quantity, $\phi(t)$, varies between zero just before contact and unity at long times, once asperity junctions no longer grow in size and number.

Sliding on impermeable, hard surfaces. We observed previously that the value of μ for a finger pad sliding on a smooth glass surface also increased with the contact time because the increase in A_{true} is greater than the decrease in τ [20]. The value of μ can increase by up to an order of magnitude for small normal loads and its evolution at a constant normal load can be described by a first-order kinetics relationship with a characteristic time of up to 20 s [29]. Thus it is probable that $\phi(t)$ generally exhibits a similar behaviour but a technique able to reliably measure A_{true} for rough surfaces has yet to developed. We also previously reported that with increasing contact time, the friction of a finger pad gradually changes from Coulombic to a nonlinear dependence on a normal load, in a manner that is typical of elastomers, when the asperities are sufficiently compliant to flatten under the applied load [29]. This phenomenon is a direct result of a glassy-rubbery transition of the *stratum corneum* due to the moisture-driven plasticisation. Thus, in the fully occluded state, $A_{\mathrm{true}} \approx A_{\mathrm{junct}}$.

Sliding on soft surfaces. The surprisingly slow formation of a true contact between a finger pad and a hard, smooth, and

impermeable surface, such as glass, may be contrasted with the case of a counter surface made of a compliant material, such as a rubber or an elastomer (e.g. PDMS), as further illustrated by the 'true contact' images in Fig. 4a that were acquired with the same finger tested under similar conditions but with a different material. Figure 4b shows the evolution of the coefficient of friction, μ, when a finger pad slid on a smooth elastomeric surface (PDMS: Young's elastic modulus $E = 2.3\,\mathrm{MPa}$; estimated Young's elastic modulus of keratin: $E \approx 1\,\mathrm{GPa}$ in a dry state) and on a glass surface. For PDMS, the coefficient of friction was nearly constant throughout the contact time, while a first-order kinetic relationship of the form of [**1**] could be successfully fitted in the case of a glass surface.

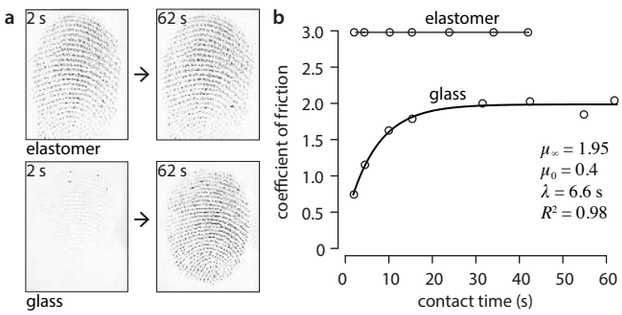

Fig. 4. (**a**) Contrasted kinetics of contact formation for a peak compression of 2 N, showing images at the beginning and end of the subsequent hold period. (**b**) Time course of the evolution of friction for a finger sliding on an elastomeric surface or on a glass surface (fitted to a first-order kinetic relationship) at a velocity of $0.02\,\mathrm{m\,s^{-1}}$ and under a load of 0.2 N.

The greyscale images in Fig. 4a show a few dark spots that may be ascribed to the presence of water droplets. This possibility raises the concern that our analysis of the true contact area may have been be confounded by the occurence of water bridges in interstitial spaces that would cause an overestimation of the true contact area. The presence of water, however, could not explain the increase of the coefficient by a factor five over a period of 20 s as shown by Fig 4b. Moreover, free moisture would be expected to lead to a reduction of the friction.

Implications for the motor and the perceptual functions of touch. The dramatic differences in true contact formation kinetics according to the material properties and to the microtopology of the counter surface has obvious implications for motor behaviour. We intuitively feel that elastic rubbery surfaces, even if they are only thin coatings, provide us with a better grip than hard and smooth surfaces. Conversely, the kinematic and tonic motor behaviour required to explore surfaces is crucially dependent on the nature of these surfaces. Push too hard on a surface made of a compliant material and the finger will become stuck. Conversely, clean glass surfaces will remain slippery within the first ten seconds of contact regardless of their topology, especially in dry ambient conditions. Each of these cases requires fine and flexible motor control strategies for the successful completion of motor or perceptual tasks. The kinetics of true contact formation are also likely to be impacted by the hydrophobicity of the material of the counter surface. In fact, we have recently shown that people can discriminate materials by touch on the sole basis of hydrophobicity differences [6]. We thus can tentatively suggest that the contact formation kinetics divide the tactile world into broad categories of materials: smooth and impermeable surfaces that could be subdivided into those that are hard (glass, glazings, polished metals) or those that are softer than keratin (rubbers, certain polymers); rough surfaces can also be divided into those that are made of relatively hard and soft materials; and porous surfaces (paper, wood, fabrics) that further modify the kinetics of contact formation together with hydrophobicity. For example, it has been observed that for filter paper the friction, and hence A_{true}, reduces with the contact time since the secreted sweat is absorbed, leading to reduction in the compliance of the keratin [2]. It can therefore be argued that each of these factors potentially convey reliable tactile information to the brain pertaining to the nature of the touched objects during tactile exploration.

Implications for tactile displays relying on friction. The modulation of friction by the application of ultrasonic vibration or by electrostatic adhesion is a leading technological option for flat screen haptic displays [30, 31]. They rely on the ability to reduce or augment the overall friction of the screen. The illusion of a ridge [32] may be created by rapidly increasing friction during the exploration by a finger as a result of decreasing the amplitude of vibration or increasing the electrostatic field [3]. The strength and stability of this effect is dependent on the contrast in friction that can be induced, which has critical implications for power requirements [33, 34]. The drastic variations of the evolution of A_{junct} with contact time as was observed here for just two participants in a single day is indicative of the variations that might typically be expected for the corresponding intrinsic friction of touch screens. This variation extends to the increase in μ with time while the data for the glass in Fig. 4b correspond to an increase of about a factor of five. Our findings are indeed consistent with the variations in reported values of the coefficient of friction that are reported in the literature [2, 35, 36]. Thus if the intrinsic friction between a finger pad and screen is small, greater vibrational amplitudes or greater electrostatic voltage swings will be required. Clearly, our findings present a significant challenge to the design of haptic interfaces based on friction modulation in terms of maintaining acceptable fidelity without excessive power requirements.

Materials and Methods

Data Acquisition. The experimental platform used to measure the time evolution of the contact area under an applied normal load is shown schematically Fig. 5a. High contrast images can be obtained directly using the FTIR technique and thus be rendered in a variety of ways other than binary images. An example is shown in Fig. 5b.

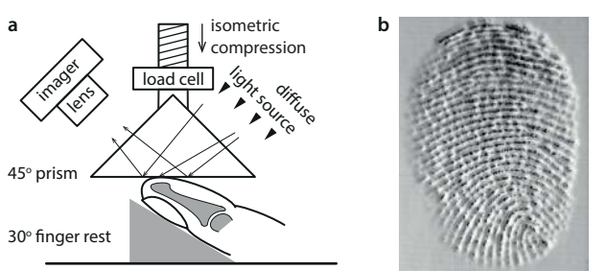

Fig. 5. (**a**) Schematic diagram of the FTIR technique employed to measure the contact area between a finger pad and a glass prism. Light rays are entirely reflected unless there is intimate contact resulting in a dark image against a light background. (**b**) 3D grey-scale rendering of a finger print image.

The left index finger of two female volunteers (27 and 26 years old), who gave informed consent and who are denoted as participants A and B, was inclined at angle of 30° with the finger pad facing upwards. A flat glass prism was pressed down onto the finger pad in order to induce frustrated total internal reflection, while the contact area increased by the applied load. For the elastomer contact studies, a smooth transparent block of PDMS (Sylgard 184) was adhered to the lower rectangular face of the prism. Initially, the fingers were washed with commercial soap, rinsed with distilled water and allowed to dry for 10 min until an equilibrated clean skin state was achieved. The rear face of the prism was backlit uniformly by reflecting light from a fibre-optic lamp with a diffusely reflecting white surface. The contact was imaged through the front face of the prism using a Nikon D5300 camera with a video resolution of 1920 x 1080 pixels at 25 fps and a shutter speed of 1/160 s. The camera was fitted with a macro lens and a small aperture was used to achieve the depth of field necessitated by oblique viewing. It was fixed to the moving crosshead of the machine and focused on the centre of the lower prism surface.

The images obtained were high-contrast patterns of dark ridges where the light was scattered into a bright background where the light was completely reflected. The compression of the finger pad was conducted at rates of 0.5, 1, and 2 mm s^{-1} until a load of 2 or 3 N was reached (the testing parameters for each participant are listed in Table 1). The prism was attached to a Universal Materials Testing Machine (model no. 5566, ex Instron, UK) via a 10 N transducer. The displacement of the prism was then maintained for 60 s before unloading the contact at the same rate. The compressive force and displacement data were recorded at 500 Hz. To ensure that accidental slip did not take place during imaging, additionally image and force data analysis was performed. Any such slip would have been indicated by abrupt changes in the evolution of the number of junctions and in the normal load. All measurements apart from those associated with Fig. 4a were carried out in a single day and in an environmentally controlled laboratory set to 20°C and 50% relative humidity.

Image processing. Using the ImageJ software [37], image analysis was carried out to determine A_{junct} as a function of the contact duration. Grey scale (8-bit) conversion and analysis was applied. The converted images were adjusted to the level of contrast and brightness that allowed for optimal pattern recognition. Typical methods were adopted for automatic fingerprint feature extraction [38] and followed a sequence of steps comprising: image enhancement, binarisation, thinning, extraction, and post-processing. It was possible to exclude the sweat pores and to determine the size and evolution of each feature by segmenting the image into features of interest from the background under each relevant condition by use of a mask function. To estimate A_{junct} a threshold of the grey scale value was determined from the histogram ($> 75\%$ saturation of the pixel intensities), that allowed the boundaries of the contact junctions to be delineated. The boundary of each junction excluded sweat pores at the edge of the contact region but it was not possible to exclude automatically those that were internal to the boundaries. It was estimated that the overestimation of the contact area was $< 5\%$ since such internal sweat pores represented a relatively small proportion of the total contact area particularly because they were only present in the central region of the fingerprint image.

ACKNOWLEDGMENTS.
This study was funded by the FP7 Marie Curie Initial Training Network PROTOTOUCH, grant agreement No. 317100. It was also supported by the European Research Council (FP7) ERC Advanced Grant (PATCH) to V.H. grant agreement No. 247300.

1. Dyson J & Hirst W (1954) The true contact area between solids. Proc Phys Soc B 67:309–312.
2. Pasumarty SM, Johnson SA, Watson SA, Adams MJ (2011) Friction of the human finger pad: influence of moisture, occlusion and velocity. Tribol Lett 44:117–137.
3. Vezzoli E, Messaoud WB, Amberg M, Giraud F, Lemaire-Semail B, Bueno MA (2015) Physical and perceptual independence of ultrasonic vibration and electrovibration for friction modulation. IEEE Trans Haptics 8:235–239.
4. Wiertlewski M, Friesen RF, Colgate JE (2016) Partial squeeze film levitation modulates fingertip friction. Proc Natl Acad Sci U S A 113:9210–9215.
5. Nakatani M, Howe RD, Tachi S (2011) Surface texture can bias tactile form perception. Exp Brain Res 208:151–156.
6. Gueorguiev D, Bochereau S, Mouraux A, Hayward V, Thonnard JL (2016) Touch uses frictional cues to discriminate flat materials. Sci Rep 6:25553.
7. McKittrick J, Chen PY, Bodde SG, Yang W, Novitskaya EE, Meyers MA (2012) The structure, functions, and mechanical properties of keratin. JOM 64:449–445.
8. Dzidek BM, Adams MJ, Andrews JW, Zhang Z, Johnson SA (2017) Contact mechanics of the human finger pad under compressive loads. J R Soc Interface 14(127):20160935.
9. Wildnauer RH, Bothwell JW, Douglass AB (1971) Stratum corneum biomechanical properties, I. Influence of relative humidity on normal and extracted human stratum corneum. J Invest Dermatol 56:72–78.
10. Lévesque V, Hayward, V (2003) Experimental evidence of lateral skin strain during tactile exploration. EuroHaptics pp 261–275.
11. Tada M, Mochimaru M, Kanade, T (2006) How does a fingertip slip?—visualizing partial slippage for modeling of contact mechanics. EuroHaptics pp 415–420.
12. Warman PH, Ennos AR (2009) Fingerprints are unlikely to increase the friction of primate fingerpads. J Exp Biol 212:2015–2021.
13. Adams MJ, Johnson SA, Lefèvre P, Lévesque V, Hayward V., André T, Thonnard, JL (2013) Finger pad friction and its role in grip and touch. J R Soc Interface 10(80):20120467.
14. André T, Lefèvre P, Thonnard JL (2009) A continuous measure of fingertip friction during precision grip. J Neurosci Methods 179:224–229.
15. André T, Levèsque V, Hayward V, Lefèvre P, Thonnard JL (2011) Effect of skin hydration on the dynamics of fingertip gripping contact. J R Soc Interface 8(64):1574–1583.
16. Delhaye B, Lefèvre P, Thonnard JL (2014) Dynamics of fingertip contact during the onset of tangential slip. J R Soc Interface 11(100):20140698.
17. Terekhov AV, Hayward, V (2011) Minimal adhesion surface area in tangentially loaded digital contacts. J Biomech 44(13):2508–2510.
18. Soneda T, Nakano K (2010) Investigation of vibrotactile sensation of human finger pads by observation of contact zones. Tribol Int 43:210–217.
19. Bochereau S, Dzidek B, Adams MJ, Hayward V (2017) Characterizing and imaging gross and real finger contacts under dynamic loading. IEEE Trans Haptics in press.
20. Dzidek BM, Bochereau S, Johnson SA, Hayward V, Adams MJ (2016) Frictional dynamics of finger pads are governed by four length-scales and two time-scales. Haptics Symposium pp 161–166.
21. Pawluk DTV, Howe RD (1999) Dynamic contact of the human fingerpad against a flat surface. J Biomech Eng 121:605–611.
22. Dąbrowska AK, Adlhart C, Spano F, Rotaru GM, Derler S, Zhai L, Spencer ND, Rossi RM (2016) In vivo confirmation of hydration-induced changes in human-skin thickness, roughness and interaction with the environment. Biointerphases 11:031015.
23. Amuzu JKA, Briscoe BJ, Tabor D (1977) Friction and shear strength of polymers. ASLE Trans 20(4):354–358.
24. Briscoe BJ, Arvanitaki A, Adams MJ, Johnson SA (2001) The friction and adhesion of elastomers. Tribol Series 39:661–672.
25. Briscoe BJ, Smith AC. (1981) Polymer friction and polymer yield: a comparison. Polymer. 22:1587–1589.
26. Cohen SC, Tabor D. (1966) The friction and lubrication of polymers. Proc. Roy. Soc. Lond. A 291: 186–207.
27. Johnson SA, Gorman DM, Adams MJ, Briscoe BJ (1993) The friction and lubrication of human stratum corneum. Tribol Series 25:663–672.
28. Adams MJ, Briscoe BJ, Johnson SA (2007) Friction and lubrication of the human skin. Tribol Lett 26:239–253.
29. Dzidek BM, Adams MJ, Zhang Z, Johnson SA, Bochereau S, Hayward, V (2014) Role of occlusion in non-Coulombic slip of the finger pad. Haptics: Neuroscience, Devices, Modeling, and Applications pp 109-116.
30. Giraud F, Amberg M, Lemaire-Semail B, Casiez G (2012) Design of a transparent tactile stimulator. Symposium on Haptic Interfaces For Virtual Environment And Teleoperator Systems pp 485–489.
31. Meyer D, Peshkin M, Colgate JE (2013) Fingertip friction modulation due to electrostatic attraction. World Haptics Conference pp 43–48.
32. Robles De La Torre G, Hayward V (2001) Force can overcome object geometry in the perception of shape through active touch. Nature 412(6845):445–448.

33. Vezzoli E, Vidrih Z, Giamundo V, Lemaire-Semail B, Giraud F, Rodic T, Peric D, Adams M Friction reduction through ultrasonic vibration part 1: modelling intermittent contact. IEEE Trans Haptics in press.
34. Sednaoui T, Vezzoli E, Dzidek B, Lemaire-Semail B, Chappaz C, Adams M Friction reduction through ultrasonic vibration part 2: experimental evaluation of intermittent contact and squeeze film levitation. IEEE Trans. Haptics in press.
35. Derler S, Rotaru GM (2013) Stick-slip phenomena in the friction of human skin. Wear 301:324–329.
36. Urbakh M, Klafter J, Gourdon D, Israelachvili J (2004) The nonlinear nature of friction. Nature, 430(6999):525-528.
37. https://imagej.net
38. Domeniconi C, Tari S, Liang P (1998) Direct gray scale ridge reconstruction in fingerprint images. IEEE Int. Conf. Acoustics Speech and Signal Processing pp V-2941.